Molecules and Cells

Time-Lapse Live-Cell Imaging Reveals Dual Function of Oseg4, *Drosophila* WDR35, in Ciliary Protein Trafficking

Nayoung Lee[1], Jina Park[1,4], Yong Chul Bae[2], Jung Ho Lee[3], Chul Hoon Kim[3], and Seok Jun Moon[1,*]

[1]Department of Oral Biology, BK21 PLUS, Yonsei University College of Dentistry, Seoul 03722, Korea, [2]Department of Oral Anatomy and Neurobiology, BK21, School of Dentistry, Kyungpook National University, Daegu 41940, Korea, [3]Department of Pharmacology, Yonsei University College of Medicine, Seoul 03722, Korea, [4]Laboratory of Low Dose Risk Assessment, National Radiation Emergency Medical Center, Korea Institute of Radiological & Medical Sciences, Seoul 01812, Korea
*Correspondence: sjmoon@yuhs.ac
http://dx.doi.org/10.14348/molcells.2018.0179
www.molcells.org

Cilia are highly specialized antennae-like organelles that extend from the cell surface and act as cell signaling hubs. Intraflagellar transport (IFT) is a specialized form of intracellular protein trafficking that is required for the assembly and maintenance of cilia. Because cilia are so important, mutations in several IFT components lead to human disease. Thus, clarifying the molecular functions of the IFT proteins is a high priority in cilia biology. Live imaging in various species and cellular preparations has proven to be an important technique in both the discovery of IFT and the mechanisms by which it functions. Live imaging of *Drosophila* cilia, however, has not yet been reported. Here, we have visualized the movement of IFT in *Drosophila* cilia using time-lapse live imaging for the first time. We found that NOMPB-GFP (IFT88) moves according to distinct parameters depending on the ciliary segment. NOMPB-GFP moves at a similar speed in proximal and distal cilia toward the tip (~0.45 μm/s). As it returns to the ciliary base, however, NOMPB-GFP moves at ~0.12 μm/s in distal cilia, accelerating to ~0.70 μm/s in proximal cilia. Furthermore, while live imaging NOMPB-GFP, we observed one of the IFT proteins required for retrograde movement, Oseg4 (WDR35), is also required for anterograde movement in distal cilia. We anticipate our time-lapse live imaging analysis technique in *Drosophila* cilia will be a good starting point for a more sophisticated analysis of IFT and its molecular mechanisms.

Keywords: *Drosophila*, intraflagellar transport, live imaging, *Oseg4*, primary cilia

INTRODUCTION

Cilia are highly specialized antennae-like organelles that extend from the apical surface of many of cells in the human body (Ishikawa and Marshall, 2011). Cilia are essential for many developmental signaling pathways and for adult homeostasis (Berbari et al., 2009; Singla and Reiter, 2006). Defects in ciliary function result in a wide range of diseases called ciliopathies. These include polycystic kidney disease, retinitis pigmentosa, Bardet-Biedel syndrome, and Joubert syndrome (Green et al., 1989; Liu et al., 2002; Pazour et al., 2000; Valente et al., 2006).

Cilia are composed of a microtubule-based core structure called the axoneme, which is surrounded by a ciliary membrane that is continuous with the plasma membrane. Because most protein synthesis is restricted to the cytoplasm, the biogenesis and maintenance of cilia requires an elaborate import and export system called intraflagellar transport (IFT) (Cole et al., 1998; Scholey and Anderson, 2006). Kinesin-2-driven anterograde IFT delivers ciliary precursors and signaling molecules to the tips of cilia (Cole et al.,

Received 2 April, 2018; revised 1 June, 2018; accepted 4 June, 2018; published online 9 July, 2018

eISSN: 0219-1032

1998), and dynein-driven retrograde IFT returns ciliary components to the bases of cilia (Pazour et al., 1998).

Analysis of immunostained cilia after cellular fixation has improved our understanding of the molecular underpinnings of IFT, but many ciliary proteins are in constant motion. Thus, the imaging of living cells is central to the discovery of the molecular mechanisms of IFT. Although live imaging of individual IFT components has been performed in a variety of ciliated organisms, (e.g., Chlamydomonas, *C. elegans*, *Trypanosoma brucei*, Xenopus, and mammals) (Buisson et al., 2013; Engel et al., 2009; Follit et al., 2006; Iomini et al., 2001; Lechtreck et al., 2009; Snow et al., 2004; Tran et al., 2008; Williams et al., 2014), we are not aware of any studies using live imaging to examine IFT in *Drosophila melanogaster*.

Here, we investigate IFT motility parameters in *Drosophila* for the first time. We established a protocol for the live imaging of cilia in the chordotonal neurons of the Johnston's organ (JO), which flies use to hear. We then used this protocol to investigate the motion of a GFP-tagged homolog of IFT88, NOMPB-GFP. The cilia of the chordotonal neurons are divided into structurally distinct proximal and distal ciliary segments (Fig. 1A) (Moulins, 1976; Uga and Kuwabara, 1965). We find anterograde IFT trains move at similar speeds in proximal and distal cilia, but retrograde IFT trains move at different speeds. We also demonstrate that mutations of the IFT-A complex component Oseg4 (WDR35) abolishes anterograde IFT movement in distal cilia and retrograde IFT movement in both ciliary segments. Together, we demonstrate that live imaging of *Drosophila* cilia facilitates the measurement of the motility parameters of various IFT components and permits the visualization and comparison of the dynamics of IFT motility in wild-type and mutant cilia.

MATERIALS AND METHODS

Fly stocks

rempA^{1}, *btv*^{5P1}, *IAV-GFP*, *REMPA-YFP*, *NOMPB-GFP* and *UAS-mCD8:GFP* were previously described (Jeong et al., 2016; Park et al., 2013). All fly stocks were grown on conventional cornmeal agar molasses media.

In vivo Live Imaging Analysis

Live imaging of IFT movements was performed by mounting dissected late pupal-stage antennae in Schneider's insect medium (Life Technologies, Gibco, cat. no. 21720-024-500 ml) supplemented with 10% FBS (Life Technologies, Gibco, cat. no. 10099-141-500 ml), 1% antibiotic-antimycotic solution (Sigma-Aldrich, cat. no. A5955), and 0.2 mg/ml insulin (10 mg/ml; Sigma-Aldrich, cat. no. i9278-5 ml). Samples were covered with 24 × 50 mm cover glasses (Marienfeld, High Precision No. 1.5H, 107222). Vaseline was added to each coverslip to maintain a space for the samples. Samples were imaged on a Zeiss LSM 780 confocal microscope with GaAsp detectors, and a 63 × 1.4 numerical aperture oil-immersion objective at 600 ms per frame for 1 min at room temperature (21℃). Fluorescence recovery after photobleaching (FRAP) analysis was performed by making a pre-bleaching fluorescence measurement for 6 seconds, photobleaching with repeated full-power pulses of a 488 nm laser for 3 s, and then imaging the fluorescence recovery every 600 ms for 54 s. The number of cilia measured in each experiment is noted in Table 1 for each strain. ImageJ was used with the Kymograph Clear macro toolset to generate kymographs from streaming videos of cilia and to manually trace lines on moving particles (Mangeol et al., 2016). The resulting kymographs and traced lines were analyzed using the Kymograph direct software to calculate the velocity of each moving particle (Mangeol et al., 2016).

Generation of *Oseg4*^{1} mutant flies

Ends-out homologous recombination (Gong and Golic, 2003) was used to generate the *Oseg4*^{1} mutant flies. The *Oseg4*^{1} allele was made using 3 kb arms from the 5' and 3' ends of the *Oseg4* coding region (179-1043) PCR-amplified from *w*^{1118} and then sub-cloned into the pw35 vector. The primers for the 5' homologous arm of the resulting pw35 vector are 5'-GCGGCCGCACTAAAAAATACCAACTGCTCAGGCG-3' and 5'-GCATGCCTTGGAGTTGCAAGTGCACTTGG-3'. The primers for the 3' homologous arm of the resulting pw35 vector are 5'-GGTACCGCTGTAAGTTAGTACTTGATTATCC-3' and 5'-GGATCCTCGTACCGTTGAAGGGTAGCC-3'. The deletion of *Oseg4* coding regions was confirmed by genomic PCR using the following primers were used to confirm the *Oseg4*^{1} mutant flies: 5'-CATCGCTTGGAATAAGGAGGAG-3' and 5'-GGGTCTGGTTCATCGACAAAT-3'.

Generation of transgenic flies

To generate the *Nan-GAL4* allele, we used a 2 kb promoter fragment located upstream of the first exon of nanchung. The primers for the pCaSpeR4*GAL4* vector are 5'-GGTACCCTGTTGAAATATATTTGCGTATCCAATTGG-3' and 5'-GCGGCCGC-CATTATCCGATCCCAAATTCACTC-3'. A 644 bp promoter fragment located upstream of the first exon of *Oseg4* was used to generate *Oseg4-GAL4*. The primer sequences for the pCaSpeR4*GAL4* vector are 5'-GGTACCTATCCCCCGCGTGCCCTG-3' and 5'-GCGGCCGCCATCTTGGAGTTGCAA. A full-length *Oseg4* cDNA clone was amplified from *Drosophila* Gold Collection LD29485 from *Drosophila* Genome Resource Center and sub-cloned into the pUAST vector to generate the UAS-Oseg4 transgenic fly.

Electrophysiology

Extracellular electrophysiology in fly antennae was performed using computer-generated pulse songs as previously described (Eberl et al., 2000). After inserting a reference electrode in the dorsal head, a recording electrode was inserted between the first and second antennal segments. A DAM50 differential amplifier (World Precision Instruments, USA) was used for signal extraction and the Superscope 3.0 software (GW Instruments, USA) was used for signal digitization. Each sound-evoked potential represents the average response to 10 stimuli.

Cryosections

CO_2-anesthetised adult Drosophila heads were embedded in base molds (#M475-4, Simport Scientific, Canada) using Tissue-Tek O.C.T. compound (Sakura Finetek Europe B.V., Alphen aan den Rijn, The Netherlands) and frozen on an

aluminum block pre-cooled in liquid nitrogen. Using a Leica CM3050 S cryostat (Nussloch, Germany), the embedded samples were mounted on an object holder and sectioned. 14 μm sections were collected from each frozen block and mounted on Superfrost microscope slides.

Immunohistochemistry

For fluorescence immunostaining, antennae were prepared from pupal stage flies but all other samples were prepared from adult stage flies. First, the slides with cryosectioned specimens and dissected tissues were fixed with 4% paraformaldehyde in 1X PBS containing 0.2% TritonX-100 (PBS-T) for 10 or 20 min. After washing 3 times with PBS-T, the tissues were blocked with 5% heat-inactivated goat serum in PBS-T for 1 h. The tissues were then incubated with primary antibodies in the same blocking solution overnight at 4℃. After washing 3 times with PBS-T, the tissues were incubated with secondary antibodies (this study;1:400 dilution) in PBS-T for 1 h at room temperature and washed three times with PBST. After washing, the samples were mounted in Vectashield (Vector Laboratories, USA) and examined using a Zeiss LSM700 confocal microscope (Jena, Germany). When comparing the localization and expression level of ciliary proteins between the control and experimental groups, all samples were prepared at the same time and all confocal images were obtained under the same conditions and settings.

Antibodies

Fragments encoding NOMPA (amino acids 451-592) conjugated to GST were injected into rats to produce rat NOMPA antibodies. The primary antibodies used in this study were diluted as follows: rabbit anti-NOMPC, 1:400; rabbit anti-REMPA, 1:500; rabbit anti-GFP, 1:1000 (Molecular Probes, Eugene, OR); rat anti-NOMPA, 1:500. The secondary antibodies used in this study are as follows: Alexa 488-, Alexa

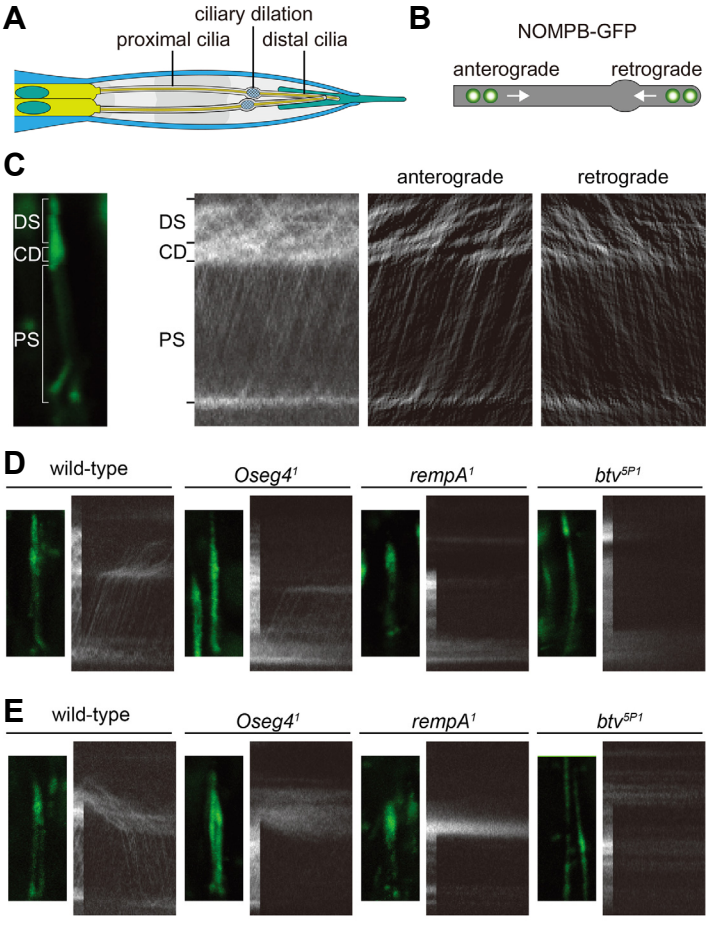

F

NOMPB-GFP average velocity (μm/sec)

	anterograde motility				retrograde motility			
	PS	n	DS	n	PS	n	DS	n
wild-type	0.45±0.01	82	0.43±0.03	21	0.70±0.02	45	0.12±0.01	11
Oseg4¹	0.44±0.01	108	none/few		none		0.06±0.01	17
rempA¹	none				none			
btv5P1	none		none		none		none	

Fig. 1. *In vivo* imaging of NOMPB-GFP in wild-type, *Oseg4¹*, *rempA¹*, and *btv5P1* flies. (A) Schematic of a *Drosophila* chordotonal neuron. The compartment positions are indicated. (B) Schematic showing the movement of IFT complexes along cilia. (C) Motility of NOMPB-GFP in wild-type cilia. Shown are a representative time-averaged confocal image, a kymograph, an anterograde Fourier-filtered kymograph, and a retrograde Fourier-filtered kymograph of NOMPB-GFP. (D-E) Representative max-intensity confocal images (left) and kymographs (right) obtained from an image stack of NOMPB-GFP in *Drosophila* of the indicated genotypes. FRAP was adapted for imaging of NOMPB-GFP movements. (D) Anterograde movement of NOMPB-GFP. Whole cilia, except for the basal part, were photobleached. (E) Retrograde movement of NOMPB-GFP. Whole cilia, except for their ciliary tips, were photobleached. (F) NOMPB-GFP average velocities along the chordotonal cilia of wild-type, *Oseg4¹*, *rempA¹*, *btv5P1* mutants. Means ± SEM are shown.

568-conjugated anti-mouse or anti-rabbit IgG (Molecular Probes; 1:400) and Texas Red conjugated anti-rat IgG (Molecular Probes; 1:400).

Transmission electron microscopy

Adult fly heads were fixed in 2% paraformaldehyde, 2.5% glutaraldehyde, 0.1 M cacodylate, and 2 mM $CaCl_2$, pH 7.4. LR white resin was used to embed the fixed samples. Embedded heads were thin sectioned, collected on formvar-coated single slot nickel grids, counterstained with uranyl acetate and lead citrate, and examined using a Hitachi H-7500 electron microscope (Hitachi, Japan).

Statistical analysis

The plots in Fig. 2F show medians ± interquartile range. Kruskal-Wallis tests with Mann-Whitney U post-hoc tests were calculated in GraphPad Prism 5. Asterisks indicate statistical significance (***$p < 0.001$, **$p < 0.01$).

RESULTS

Live imaging of *Drosophila* chordotonal cilia

To better understand IFT in *Drosophila* cilia, we established a protocol for live imaging IFT in the cilia of the JO chordotonal neuron. The JO consists of around 200 scolopidia each housing 2 or 3 chordotonal neurons (Gopfert and Robert, 2001). The cilia of the chordotonal neurons are divided into two parts, proximal and distal, by a ciliary dilation (Fig. 1A) (Moulins, 1976; Uga and Kuwabara, 1965). To investigate IFT motility parameters in *Drosophila*, we used transgenic flies harboring a GFP-tagged NOMPB, which is the *Drosophila* IFT-88 homolog. Using time-lapse microscopy, we were able to visualize both anterograde and retrograde movement of NOMPB-GFP along the length of cilia (Fig. 1B). During anterograde movement, NOMPB-GFP moves at a similar speed in proximal and distal ciliary segments (~0.44 μm/s). During retrograde movement, however, NOMPB-GFP moves in distal cilia at ~0.12 μm/s, accelerating to ~0.7 μm/s in proximal cilia (Figs. 1C and 1F).

Generation of *Oseg4* mutants

Because mutations of anterograde IFT components result in severe cilia formation defects, we decided to analyze the rate of NOMPB-GFP transport in retrograde IFT mutants in more detail. The fly genome contains four retrograde IFT components (Avidor-Reiss et al., 2004; Jékely and Arendt, 2006): REMPA (IFT140), Oseg1 (IFT122), Oseg4 (WDR35), and Oseg6 (WDR19). It also contains one retrograde motor protein for IFT, Beethoven (Dynein) (Goldstein and Gunawardena, 2000; Pfister et al., 2006; Wickstead and Gull, 2007). Because *rempA*, *Oseg1*, and *btv* mutants were available, we attempted to generate *Oseg4* and *Oseg6* mutants.

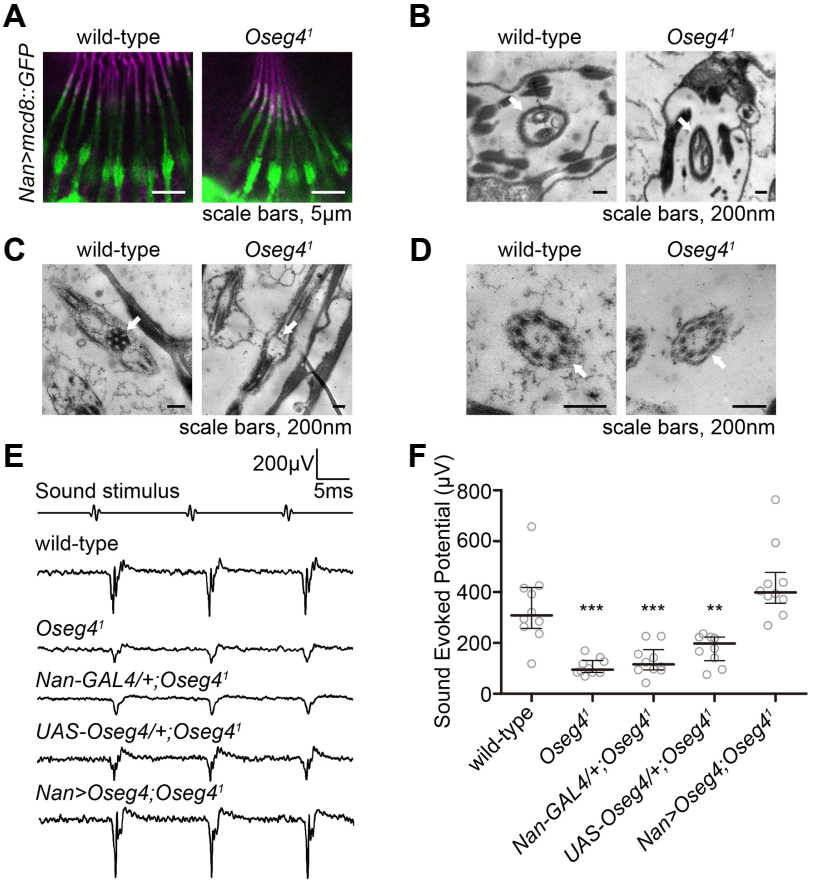

Fig. 2. Characterization of *Oseg4* mutants. (A) Confocal images of the pupal second antennal segment expressing mCD8::GFP under the control of *Nan-GAL4* in wild-type (left) and *Oseg4*^{1} mutants (right). Immunostaining of GFP (green) counterstained with NOMPA, which stains the extracellular dendritic caps (magenta). (B-D) Transmission electron microscopic examination of wild-type and *Oseg4*^{1} antennal scolopidium. Scale bars represent 200 nm. (B) Arrows indicate a cap structure. (C) Arrows indicate a ciliary dilation. (D) Arrows indicate a ciliary axoneme. (E) Representative traces of sound-evoked potentials recorded from the antennal nerves of flies of the indicated genotypes. Their hearing defects were rescued by expressing *UAS-Oseg4* in chordotonal neurons. (F) Quantifications of sound-evoked potentials. The medians and quartiles are indicated by horizontal lines. The asterisk denotes a significant reduction in sound-evoked potentials of each genotype compared with those of wild-type flies. *p* values were calculated using the Kruskal-Wallis test and Mann-Whitney *U* post-hoc tests (**$p < 0.01$, ***$p < 0.001$).

While we were unsuccessful at generating an *Oseg6* mutant, we were able to obtain via ends-out homologous recombination an *Oseg4* mutant allele containing a replacement of a 1 kb stretch of genomic DNA from the Oseg4 initiation codon with the *mini-white* coding sequence (Supplementary Fig. S1A). We confirmed deletion of the *Oseg4* coding sequence by genomic PCR (Supplementary Fig. S1B). We also observed expression of GFP driven by *Oseg4-GAL4* in ciliated sensory neurons such as the chordotonal neurons of the JO, the olfactory receptor neurons of the antennae, the gustatory receptor neurons of the labellum, and the chordotonal neurons of the femur, suggesting *Oseg4* plays a role in *Drosophila* cilia (Supplementary Fig. S1C).

The requirement of Btv and IFT-A components for NOMPB-GFP trafficking

Using live imaging, we examined NOMPB-GFP movement in the JO neurons of *Oseg4*^{1}, *rempA*^{1}, and *btv*^{5P1} flies. We employed the Fluorescence Recovery After Photobleaching (FRAP) technique to more clearly investigate the movement of NOMPB-GFP (Figs. 1D and 1E). *Oseg4*^{1} flies did not show any significant difference from wild-type in the anterograde movement of NOMPB-GFP in proximal cilia, but we observed little to no anterograde movement in distal cilia or retrograde movement in proximal cilia (Figs. 1D-1F). In addition, retrograde motion in distal cilia was half the speed of that of wild-type cilia. In contrast, *rempA*^{1} flies, whose cilia only have proximal segments, and *btv*^{5P1} flies, which lack ciliary dilations, show no movement of NOMPB-GFP at all (Figs. 1D-1F). Together, these results suggest Oseg4 is required for anterograde movement in distal cilia and retrograde movement in both proximal and distal cilia, and this pattern is distinct from that of REMPA and Btv (Figs. 1D-1F).

Ultrastructural analysis of chordotonal neuron cilia

To investigate the role of Oseg4 in cilia in more detail, we examined whether *Oseg4*^{1} mutants have structural defects in cilia. We observed the expression of a membrane-tethered GFP driven by *Nan-GAL4* (Jeong et al., 2016) in Johnston's organ chordotonal neurons. We did not observe any differences in the number, shape, or length of cilia of *Oseg4*^{1} chordotonal neurons compared with those of wild-type chordotonal neurons (Fig. 2A). Electron microscopy of the JO revealed no paracrystalline inclusions in the ciliary dilations of *Oseg4*^{1} flies, which is reminiscent of the *btv*^{5P1} mutant phenotype (Fig. 2C) (Eberl et al., 2000). Despite their lack of paracrystalline inclusions, however, the doublet microtubules of the 9+0 cilium (Fig. 2D) and the ciliary cap connection (Fig. 2B) seem normal. These results suggest Oseg4 has a function similar to Btv in the formation of the ciliary dilation.

Loss of Oseg4 impairs hearing

To determine whether loss of Oseg4 in the JO affects *Drosophila* hearing, we recorded extracellular sound-evoked potentials in wild-type and *Oseg4*^{1} flies. *Oseg4*^{1} flies show sound-evoked potentials one-third the size of those of wild-type flies (Figs. 2E and 2F). Introduction of a wild-type *Oseg4* cDNA in the *Oseg4* mutant background under the control of *Nan-GAL4* rescues the hearing defect of *Oseg4*^{1} flies, suggesting their hearing defect can be attributed to the loss of *Oseg4* in the JO neurons.

Oseg4 is required for proper ciliary protein localization

To further understand the role of Oseg4 in the JO neurons, we examined the ciliary localization of IFT and ciliary cargo proteins in fixed JO neurons. First, we investigated the localization of the IFT proteins NOMPB and REMPA (Fig. 3). NOMPB is a component of the IFT-B complex that localizes to whole cilia with extra accumulation in the ciliary dilation and ciliary base. *Oseg4*^{1} show abnormal NOMPB-GFP accumulation in cilia accompanied by a dramatic increase in accumulation at the ciliary dilation (Fig. 3A). REMPA is a component of the IFT-A complex that localizes to the ciliary dilations of wild-type cilia. In *Oseg4*^{1}, REMPA accumulates more in cilia, diffusing slightly from the ciliary dilations (Fig. 3B).

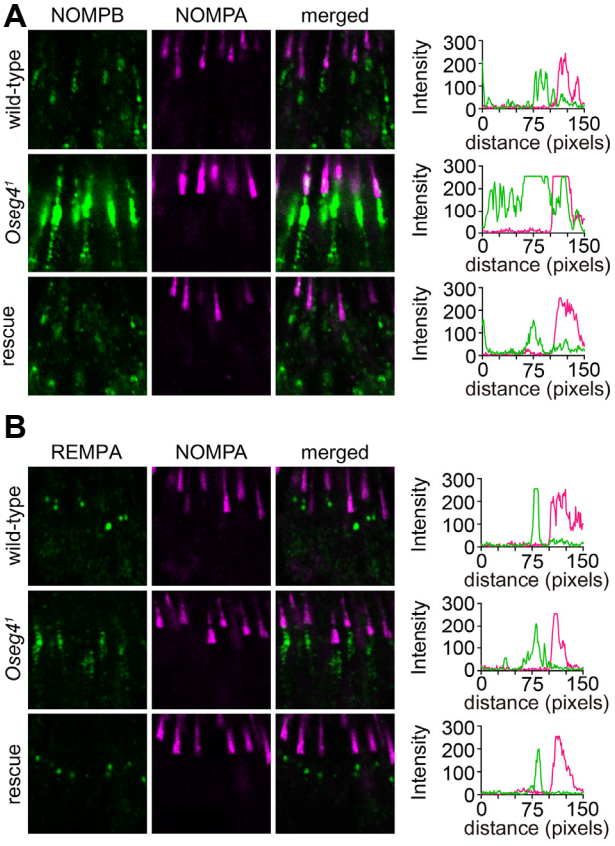

Fig. 3. Mislocalization of NOMPB and REMPA in the *Oseg4*^{1} mutant. (A, B) Confocal imaging of the second antennal segment from wild-type, *Oseg4*^{1}, and *Nan-GAL4/UAS-Oseg4;Oseg4*^{1} flies. (A) Immunostaining of NOMPB-GFP (anti-GFP) counterstained with NOMPA, which stains the extracellular dendritic cap. (left) Localization of NOMPB-GFP along cilia illustrated by intensity profile analysis (right). (B) Immunostaining of REMPA-YFP (anti-GFP) counterstained with NOMPA. (left) Localization of REMPA-YFP along the cilium illustrated by intensity profile analysis (right).

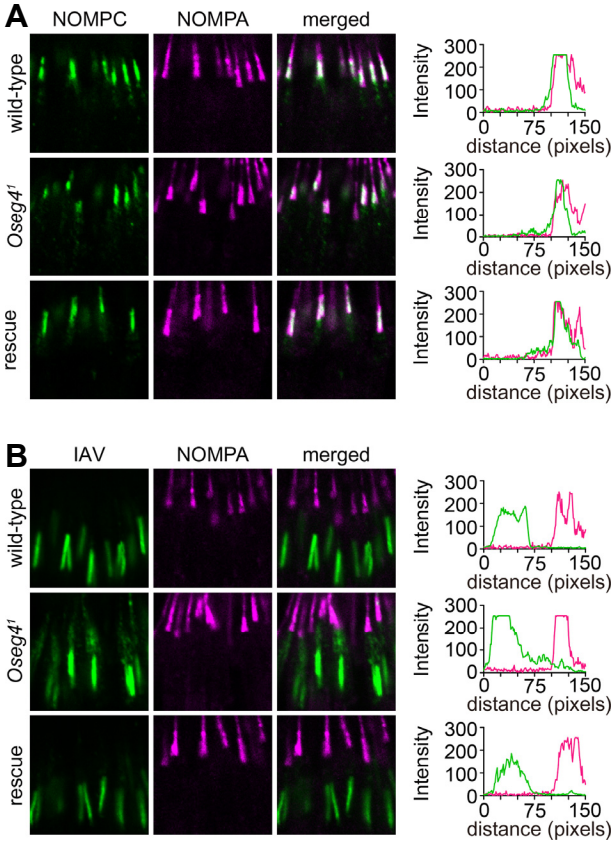

Fig. 4. Mislocalization of NOMPC and IAV in the *Oseg4*^{1} mutant. (A, B) Confocal imaging of the second antennal segment from wild-type, *Oseg4*^{1}, and *Nan-GAL4/UAS-Oseg4;Oseg4*^{1}. (A) Immunostaining of NOMPC counterstained with NOMPA. (left) Localization of NOMPC along cilia illustrated by intensity profile analysis. (right) (B) Immunostaining of IAV-GFP (anti-GFP) counterstained with NOMPA. (left) Localization of IAV-GFP along cilia illustrated by intensity profile analysis. (right)

We next tested the effect of this mislocalization of the IFT components on the ciliary localization of the ciliary cargos NOMPC and IAV (Fig. 4). Normally, NOMPC and IAV are localized in proximal and distal cilia where they play distinct roles in sound transduction and amplification, respectively. In *Oseg4*^{1} cilia, NOMPC is still localized in distal cilia but shows some skewing toward the ciliary dilation (Fig. 4A). IAV accumulates in cilia, diffusing to distal cilia (Fig. 4B). Introduction of wild-type *Oseg4* in the JO neurons of *Oseg4*^{1} using *Nan-GAL4* rescues all the localization defects of *Oseg4*^{1} cilia (Figs. 3 and 4), indicating Oseg4 has a role in normal ciliary protein trafficking.

DISCUSSION

Here, we measured IFT movement parameters in *Drosophila* cilia for the first time. Using a fast, sensitive fluorescent microscope coupled with photobleaching, we were able to clearly observe the movement of IFT complexes. Similar to *C. elegans* sensory cilia, *Drosophila* JO neuron cilia are divided into proximal and distal ciliary segments by a ciliary dilation (Fig. 1A) (Moulins, 1976; Uga and Kuwabara, 1965). In anterograde movement, NOMPB-GFP moves along proximal cilia at 0.45 μm/s, slows down in ciliary dilations, and accelerates into distal cilia (0.43 μm/s). In retrograde movement, NOMPB-GFP moves slowly in distal cilia (0.12 μm/s), accelerating into proximal cilia (0.7 μm/s). The slowdown of IFT particles in anterograde movement around ciliary dilations, which contains paracrystalline structures of unknown function, suggests their cargoes may be undergoing rearrangement. In ciliary dilations, a decision is made as to whether IFT cargo will proceed to distal cilia or return to the ciliary base. The faster movement we observed in proximal cilia with retrograde transport compared with anterograde transport and the lack of slowdown near ciliary dilations in retrograde movement implies that most ciliary cargoes simply return to the base from ciliary dilations instead of proceeding to ciliary tips.

In contrast to what we observed in *Drosophila* JO neuron cilia, IFT particles in the amphid cilia of *C. elegans* move in an anterograde direction at different rates: 0.7 μm/s along the middle segment, accelerating to 1.3 μm/s in distal segment (Snow et al., 2004). Retrograde movement in amphid cilia occurs at the same speed regardless of ciliary segment. These different IFT movement velocities in anterograde movement are created by the coordinated activity of two different IFT motors: Kinesin-II and Osm-3 (Ou et al., 2005; Pan et al., 2006; Scholey, 2013; Snow et al., 2004). It is intriguing to speculate that there is another unknown retrograde motor in addition to Btv that contributes to retrograde movement in *Drosophila*. One recent study showed depolyglutamylation in the axoneme affects anterograde IFT motor motility (Hong et al., 2018), suggesting it is possible for tubulin post-translational modifications in the two parts of the chordotonal cilia to contribute to the velocity differences we observed in retrograde movements.

In mammals, mutations in IFT-A components cause shorter or bulbous cilia (Fu et al., 2016; Liem et al., 2012; Ocbina et al., 2011; Qin et al., 2011). In *Drosophila*, while mutants in two IFT-A components—*Oseg1* (*IFT122*) and *rempA* (*IFT140*)—show truncation of their cilia to varying degrees (Avidor-Reiss et al., 2004; Lee et al., 2008), mutations of the retrograde motor *btv* induce loss of the ciliary dilation while maintaining an intact axonemal structure (Eberl et al., 2000). *Oseg4*^{1} flies phenocopy *btv* mutants in terms of the JO cilia structure, suggesting Oseg4 is involved in retrograde IFT. In addition, by applying a live imaging technique, we observed an unexpected function of Oseg4. We found that loss of Oseg4 impairs anterograde movement in distal cilia and retrograde movement in the both ciliary segments. This suggests Oseg4 plays roles in both retrograde movement and anterograde movement in distal cilia. This is further supported by evidence from fixed imaging of IFT and TRP channel cargo proteins. While we did not observe any NOMPB-GFP movement in *btv* and *rempA* mutants, presumably because retrograde movement is completely blocked, NOMPB-GFP still shows anterograde movement in proximal cilia. These data indicate Oseg4 is an accessory subunit rather than a

core subunit of IFT-A. This is consistent with a previous report studying WDR35 (Fu et al., 2016), an Oseg4 homolog. It is also possible that Oseg4 has additional roles outside of its role in retrograde IFT.

We have successfully established live imaging of IFT in *Drosophila* cilia. *Drosophila* has been suggested as an advantageous model system to study cilia not only because many genetic tools and reagents are available but also because mutations of conserved ciliary proteins do not result in embryonic lethal phenotypes that can hamper the elucidation of the molecular function of cilia *in vivo*. Combined with the advantages of the *Drosophila* model system this technique will be useful in clarifying the molecular functions of the cilia themselves. Future research on the molecular functions of the full repertoire of IFT proteins using live imaging in *Drosophila* will improve our understanding of the molecular mechanisms underlying numerous human ciliopathies.

Note: Supplementary information is available on the Molecules and Cells website (www.molcells.org).

ACKNOWLEDGMENTS

We thank the Bloomington Stock Center and Dr. M. Kernan for fly stocks. We thank the Korean Drosophila Resource Center for the generation of transgenic flies. We thank the Yonsei Advanced Imaging Center in cooperation with Carl Zeiss Microscopy, Yonsei University College of Medicine, for technical assistance. We thank the Drosophila Genomics Resource Center, supported by NIH grant 2P40OD010949 for *Oseg4* cDNA. This work was supported by a National Research Foundation of Korea (NRF) Grant funded by the Korean Government (MSIP) (NRF-2016R1A5A2008630 and NRF-2018R1A2B3001668).

REFERENCES

Avidor-Reiss, T., Maer, A.M., Koundakjian, E., Polyanovsky, A., Keil, T., Subramaniam, S., and Zuker, C.S. (2004). Decoding cilia function: defining specialized genes required for compartmentalized cilia biogenesis. Cell *117*, 527-539.

Berbari, N.F., O'Connor, A.K., Haycraft, C.J., and Yoder, B.K. (2009). The primary cilium as a complex signaling center. Curr. Biol. *19*, R526-535.

Buisson, J., Chenouard, N., Lagache, T., Blisnick, T., Olivo-Marin, J.C., and Bastin, P. (2013). Intraflagellar transport proteins cycle between the flagellum and its base. J. Cell Sci. *126*, 327-338.

Cole, D.G., Diener, D.R., Himelblau, A.L., Beech, P.L., Fuster, J.C., and Rosenbaum, J.L. (1998). Chlamydomonas kinesin-II-dependent intraflagellar transport (IFT): IFT particles contain proteins required for ciliary assembly in *Caenorhabditis elegans* sensory neurons. J. Cell Biol. *141*, 993-1008.

Eberl, D.F., Hardy, R.W., and Kernan, M.J. (2000). Genetically similar transduction mechanisms for touch and hearing in Drosophila. J. Neurosci. *20*, 5981-5988.

Engel, B.D., Ludington, W.B., and Marshall, W.F. (2009). Intraflagellar transport particle size scales inversely with flagellar length: revisiting the balance-point length control model. J. Cell Biol. *187*, 81-89.

Follit, J.A., Tuft, R.A., Fogarty, K.E., and Pazour, G.J. (2006). The intraflagellar transport protein IFT20 is associated with the Golgi complex and is required for cilia assembly. Mol. Biol. Cell *17*, 3781-3792.

Fu, W., Wang, L., Kim, S., Li, J., and Dynlacht, B.D. (2016). Role for the IFT-A Complex in Selective Transport to the Primary Cilium. Cell Rep. *17*, 1505-1517.

Goldstein, L.S., and Gunawardena, S. (2000). Flying through the drosophila cytoskeletal genome. J. Cell Biol. *150*, F63-68.

Gong, W.J., and Golic, K.G. (2003). Ends-out, or replacement, gene targeting in Drosophila. Proc. Natl. Acad. Sci. USA *100*, 2556-2561.

Gopfert, M.C., and Robert, D. (2001). Biomechanics. Turning the key on Drosophila audition. Nature *411*, 908.

Green, J.S., Parfrey, P.S., Harnett, J.D., Farid, N.R., Cramer, B.C., Johnson, G., Heath, O., McManamon, P.J., O'Leary, E., and Pryse-Phillips, W. (1989). The cardinal manifestations of Bardet-Biedl syndrome, a form of Laurence-Moon-Biedl syndrome. N Engl. J. Med. *321*, 1002-1009.

Hong, S.R., Wang, C.L., Huang, Y.S., Chang, Y.C., Chang, Y.C., Pusapati, G.V., Lin, C.Y., Hsu, N., Cheng, H.C., Chiang, Y.C., et al. (2018). Spatiotemporal manipulation of ciliary glutamylation reveals its roles in intraciliary trafficking and Hedgehog signaling. Nature Commun. *9*, 1732.

Iomini, C., Babaev-Khaimov, V., Sassaroli, M., and Piperno, G. (2001). Protein particles in Chlamydomonas flagella undergo a transport cycle consisting of four phases. J. Cell Biol. *153*, 13-24.

Ishikawa, H., and Marshall, W.F. (2011). Ciliogenesis: building the cell's antenna. Nat. Rev. Mol. Cell Biol. *12*, 222-234.

Jékely, G., and Arendt, D. (2006). Evolution of intraflagellar transport from coated vesicles and autogenous origin of the eukaryotic cilium. Bioessays *28*, 191-198.

Jeong, Y.T., Oh, S.M., Shim, J., Seo, J.T., Kwon, J.Y., and Moon, S.J. (2016). Mechanosensory neurons control sweet sensing in Drosophila. Nat. Commun. *7*, 12872.

Lechtreck, K.F., Johnson, E.C., Sakai, T., Cochran, D., Ballif, B.A., Rush, J., Pazour, G.J., Ikebe, M., and Witman, G.B. (2009). The Chlamydomonas reinhardtii BBSome is an IFT cargo required for export of specific signaling proteins from flagella. J. Cell Biol. *187*, 1117-1132.

Lee, E., Sivan-Loukianova, E., Eberl, D.F., and Kernan, M.J. (2008). An IFT-A protein is required to delimit functionally distinct zones in mechanosensory cilia. Curr. Biol. *18*, 1899-1906.

Liem, K.F., Ashe, A., He, M., Satir, P., Moran, J., Beier, D., Wicking, C., and Anderson, K.V. (2012). The IFT-A complex regulates Shh signaling through cilia structure and membrane protein trafficking. J. Cell Biol. *197*, 789-800.

Liu, Q., Zhou, J., Daiger, S.P., Farber, D.B., Heckenlively, J.R., Smith, J.E., Sullivan, L.S., Zuo, J., Milam, A.H., and Pierce, E.A. (2002). Identification and subcellular localization of the RP1 protein in human and mouse photoreceptors. Invest Ophthalmol. Vis. Sci. *43*, 22-32.

Mangeol, P., Prevo, B., and Peterman, E.J. (2016). KymographClear and KymographDirect: two tools for the automated quantitative analysis of molecular and cellular dynamics using kymographs. Mol. Biol. Cell *27*, 1948-1957.

Moulins, M. (1976). Ultrastructure of chordotonal organs. Structure and function of proprioceptors in the invertebrates. Chapman and Hall, London, 387-426.

Ocbina, P.J.R., Eggenschwiler, J.T., Moskowitz, I., and Anderson, K.V. (2011). Complex interactions between genes controlling trafficking in primary cilia. Nat. Genet. *43*, 547.

Ou, G., Blacque, O.E., Snow, J.J., Leroux, M.R., and Scholey, J.M.

(2005). Functional coordination of intraflagellar transport motors. Nature *436*, 583-587.

Pan, X., Ou, G., Civelekoglu-Scholey, G., Blacque, O.E., Endres, N.F., Tao, L., Mogilner, A., Leroux, M.R., Vale, R.D., and Scholey, J.M. (2006). Mechanism of transport of IFT particles in C. elegans cilia by the concerted action of kinesin-II and OSM-3 motors. J. Cell Biol. *174*, 1035-1045.

Park, J., Lee, J., Shim, J., Han, W., Lee, J., Bae, Y.C., Chung, Y.D., Kim, C.H., and Moon, S.J. (2013). dTULP, the Drosophila melanogaster homolog of tubby, regulates transient receptor potential channel localization in cilia. PLoS Genet. *9*, e1003814.

Pazour, G.J., Wilkerson, C.G., and Witman, G.B. (1998). A dynein light chain is essential for the retrograde particle movement of intraflagellar transport (IFT). J. Cell Biol. *141*, 979-992.

Pazour, G.J., Dickert, B.L., Vucica, Y., Seeley, E.S., Rosenbaum, J.L., Witman, G.B., and Cole, D.G. (2000). Chlamydomonas IFT88 and its mouse homologue, polycystic kidney disease gene tg737, are required for assembly of cilia and flagella. J. Cell Biol. *151*, 709-718.

Pfister, K.K., Shah, P.R., Hummerich, H., Russ, A., Cotton, J., Annuar, A.A., King, S.M., and Fisher, E.M. (2006). Genetic analysis of the cytoplasmic dynein subunit families. PLoS Genet. *2*, e1.

Qin, J., Lin, Y., Norman, R.X., Ko, H.W., and Eggenschwiler, J.T. (2011). Intraflagellar transport protein 122 antagonizes Sonic Hedgehog signaling and controls ciliary localization of pathway components. Proc. Natl. Acad. Sci. USA *108*, 1456-1461.

Scholey, J.M. (2013). Kinesin-2: a family of heterotrimeric and homodimeric motors with diverse intracellular transport functions. Annu. Rev. Cell Dev. Biol. *29*, 443-469.

Scholey, J.M., and Anderson, K.V. (2006). Intraflagellar transport and cilium-based signaling. Cell *125*, 439-442.

Singla, V., and Reiter, J.F. (2006). The primary cilium as the cell's antenna: signaling at a sensory organelle. Science *313*, 629-633.

Snow, J.J., Ou, G., Gunnarson, A.L., Walker, M.R., Zhou, H.M., Brust-Mascher, I., and Scholey, J.M. (2004). Two anterograde intraflagellar transport motors cooperate to build sensory cilia on C. elegans neurons. Nat. Cell Biol. *6*, 1109-1113.

Tran, P.V., Haycraft, C.J., Besschetnova, T.Y., Turbe-Doan, A., Stottmann, R.W., Herron, B.J., Chesebro, A.L., Qiu, H., Scherz, P.J., Shah, J.V., et al. (2008). THM1 negatively modulates mouse sonic hedgehog signal transduction and affects retrograde intraflagellar transport in cilia. Nat. Genet. *40*, 403-410.

Uga, S., and Kuwabara, M. (1965). On the Fine Structure of the Chordotonal Sensillum in Antenna of Drosophila melanogaster. J. Electron Microscopy *14*, 173-181.

Valente, E.M., Silhavy, J.L., Brancati, F., Barrano, G., Krishnaswami, S.R., Castori, M., Lancaster, M.A., Boltshauser, E., Boccone, L., Al-Gazali, L., et al. (2006). Mutations in CEP290, which encodes a centrosomal protein, cause pleiotropic forms of Joubert syndrome. Nat. Genet. *38*, 623-625.

Wickstead, B., and Gull, K. (2007). Dyneins across eukaryotes: a comparative genomic analysis. Traffic (Copenhagen, Denmark) *8*, 1708-1721.

Williams, C.L., McIntyre, J.C., Norris, S.R., Jenkins, P.M., Zhang, L., Pei, Q., Verhey, K., and Martens, J.R. (2014). Direct evidence for BBSome-associated intraflagellar transport reveals distinct properties of native mammalian cilia. Nat. Commun. *5*, 5813.